Noname manuscript No.
(will be inserted by the editor)

Hybrid Fuzzy Sliding Mode Control for Motorised Space Tether Spin-up Coupled with Axial and Torsional Oscillation

Yi Chen · **Matthew Cartmell**

Received: date / Accepted: date

Abstract A specialised hybrid controller is applied to the control of a motorised space tether spin-up space coupled with an axial and a torsional oscillation phenomenon. A seven-degree-of-freedom (7-DOF) dynamic model of a motorised momentum exchange tether is used as the basis for interplanetary payload exchange in the context of control. The tether comprises a symmetrical double payload configuration, with an outrigger counter inertia and massive central facility. It is shown that including axial and torsional elasticity permits an enhanced level of performance prediction accuracy and a useful departure from the usual rigid body representations, particularly for accurate payload positioning at strategic points. A simulation with given initial condition data has been devised in a connecting programme between control code written in $MATLAB$ and dynamics simulation code constructed within $MATHEMATICA$. It is shown that there is an enhanced level of spin-up control for the 7-DOF motorised momentum exchange tether system using the specialised hybrid controller.

Keywords fuzzy control · sliding mode control · skyhook damper · fuzzy sliding mode control · space tether

1 Introduction

Space tethers can be used for orbit raising, lowering, and maintenance, and in principle can also be used for interplanetary propulsion of appropriate payloads. The dynamics and control research on the space tether have received considerable attention by several researchers in the last few years. Alternate control laws based on the linear regulator problem were developed by Bainum et al. in 1980 [1]. A linear tension control law was provided by Kumar and Pradeep in 1998 [2]. In 1999, Pradhan, Modi and Misra [3] presented a paper which

Yi Chen
Department of Mechanical Engineering, University of Glasgow, Glasgow, G12 8QQ, UK
Tel.: +44(0)-141-330-2477
Fax: +44(0)-141-330-4343
E-mail: yichen@mech.gla.ac.uk

Matthew Cartmell
Department of Mechanical Engineering, University of Glasgow, Glasgow, G12 8QQ, UK

studied several applications of the offset scheme in controlling the tethered systems. The advantages of combining a crisp algorithmic controller and a soft knowledge-based controller were introduced by Goulet et al. in 2001 [4]. In 2003 and 2005, Barkow et al. published some papers on various methods of controlling the deployment of tethered satellites [5] [6] [7]. In 2005, Modi et al. presented their study on the development and implementation of an intelligent hierarchical controller for the vibration control of a deployable manipulator [8]. An adaptive neural control concept for the deployment of a tethered re-entry capsule was presented by Glabel et al. in 2004 [9]. A strategy for the control of the librations of a tethered satellite system in elliptic orbits using tether length control, which drives the system to controlled periodic libration trajectories was suggested by Williams in 2006 [10] [11] [12]. In 2007 and 2008, Chung, Slotine and Miller [13] [14] [15] proposed a series of papers to describe a fully decentralized linear and nonlinear control law for spinning tethered formation flight, based on exploiting geometric symmetries to reduce the original nonlinear dynamics into simpler stable dynamics.

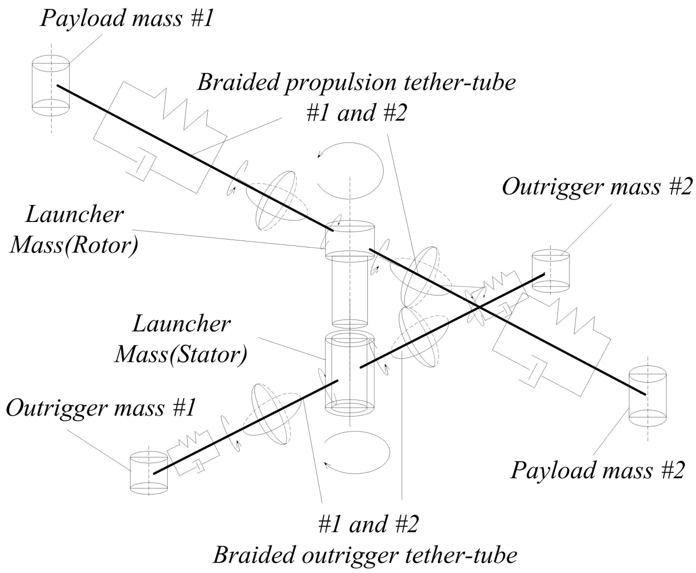

Fig. 1 Conceptual schematic of the motorised momentum exchange tether with axial and torsional elasticity

The concept of the motorised momentum exchange tether (MMET) was first proposed by Cartmell [16], and its modelling and conceptual design were developed further, in particular modelling of the MMET as a rigid body by Ziegler and Cartmell [17], and modelling of the MMET with axial elasticity by Chen and Cartmell [18]. A conceptual schematic of the MMET system with axial and torsional elasticity included is shown in Figure 1. The system is composed of the following parts: a pair of braided propulsion tether tube sub-spans, a corresponding pair of braided outrigger tether tube sub-spans, the launcher motor mass within the rotor, and the launcher motor mass within stator, the outrigger masses, and the two payload masses. The MMET is excited by means of a motor, and the model uses angular generalised coordinates to represent spin and tilt, together with an angular coordinate for circular orbital motion. Another angular coordinate defines backspin of the propulsion motor's stator components. The payload masses are fitted to each end of the tether sub-spans, and the system orbits a source of gravity in space, in this case, the Earth. The use of a tether means that all constituent parts of the system have the same angular velocity as the overall centre of mass (COM). As implied in Figure 2, the generalised coordinates of the MMET system with axial and torsional elasticity modelling are defined on orbit. The symmetrical double-ended motorised spinning tether can be applied as an orbital transfer system, in order to exploit momentum exchange for propelling and transferring payloads in space. An MMET modelling with axial and torsional elastic effects will be introduced based on the previous axial elastic MMET modelling [18] [19] [20].

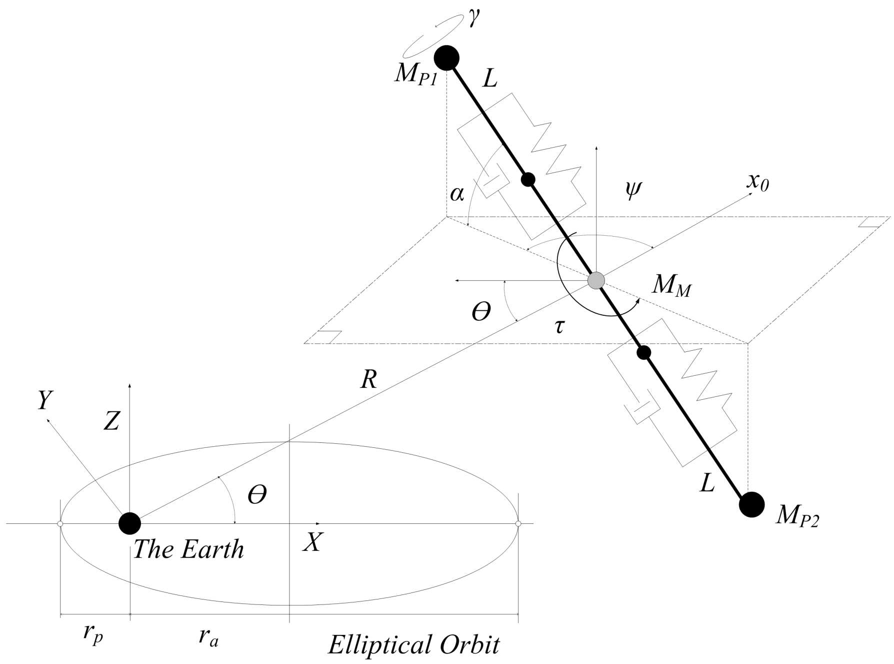

Fig. 2 Generalised coordinates of the motorised momentum exchange tether with axial and torsional elasticity, defined on orbit

It has been well recognized that fuzzy logic control (FLC) is an effective and potentially robust control method for various diverse applications The FLC rule-base is generally based on practical human experience, however, the intrinsic linguistic format expression required to construct the FLC rule base makes it difficult to guarantee the stability and robustness of the control system [21]. Variable structure control (VSC) with sliding mode control was introduced in the early 1950s by Emelyanov and subsequently published in the 1960s [22], and then further developed by several other researchers [23][24]. Sliding mode control (SMC) is recognised as a robust and efficient control method for complex, high order, nonlinear dynamical systems. The major advantage of sliding mode control is its low sensitivity to a system's parameter changes under various uncertainty conditions. Another advantage is that it can decouple system motion into independent partial components of lower dimension, which reduces the complexity of the system control and feedback design. However, a major drawback of traditional SMC is the property of chattering, which is generally disadvantageous within control systems.

In recent years, a lot of literature has been generated in the area of fuzzy sliding mode control (FSMC) [25] [26] [27] [28] [29] and has covered the chattering phenomenon of traditional SMC designs. A hybrid fuzzy skyhook surface sliding mode controller (FαSMC) [19] [20] was introduced to combine fuzzy logic control (FLC) [30] with skyhook sliding mode control (SkyhookSMC) [31] to deal with the chattering phenomenon, in which FLC is involved in designing an FαSMC-based controller. This can be harnessed to reduce the chattering problem, this feature has been applied to the design of the FαSMC controller with proper parameter selection, which can provide smooth control action and can be helpful in overcoming the disadvantages of chattering. This is why it can be useful to merge FLC with SMC to create the FSMC hybrid [29][32][33][34][35]. The hybrid fuzzy sliding mode control defined as FαSMC [19], with a skyhook surface (SkyhookSMC) is applied here to control the tether sub-span length for spin-up of the MMET system with axial and torsional elasticity.

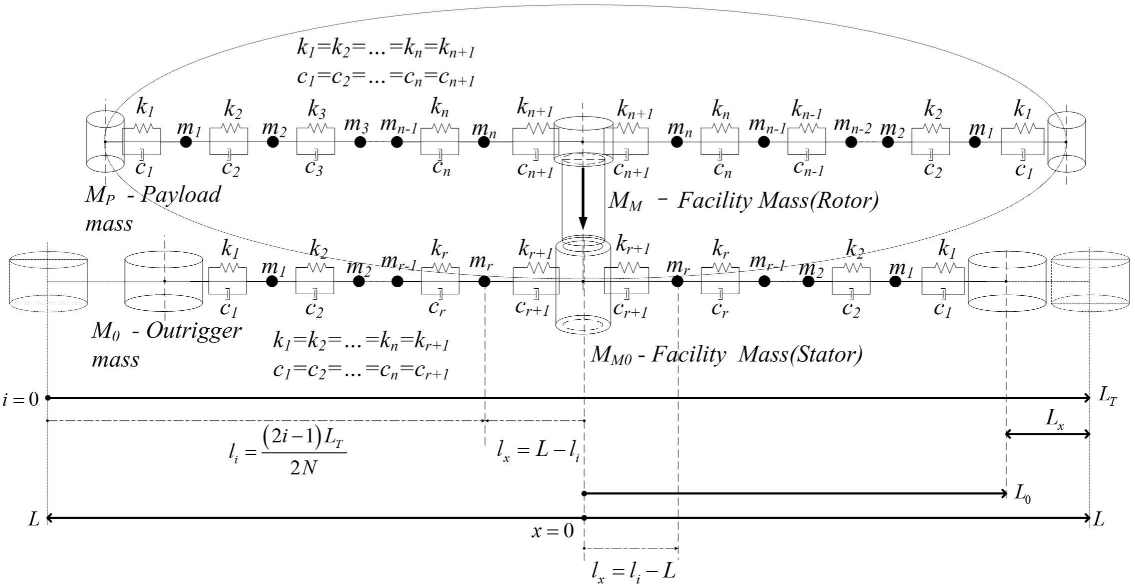

Fig. 3 Discretisation for the motorised momentum exchange tether [18]

2 Discretised MMET Model with Axial and Torsional Elasticity

A seven-degree-of-freedom (7-DOF) non-planar tether model, which includes axial and torsional elasticity coordinates, is proposed as an interim model of moderate accuracy for the MMET system. The assumptions for the elasticity modelling process are listed below:

- The tether is made of homogeneous, isotropic, elastic material–linear elastic material;
- The MMET system's dissipation function is assumed to be based on Rayleigh damping;

- The MMET is in a friction-free environment;
- Every axial ‘spring-damper’ group is connected to another, in series;
- Every torsional ‘spring-damper’ group is connected to another, in series;
- The axial, torsional and lateral elastic behaviours of the MMET tether are assumed to be independent of each other;
- There is no significant mass moment of inertia in the discretised mass points-$I_{y_{m_i}}$, so this can be ignored in this modelling context;
- The axial and torsional ‘spring-damper’ groups can be expressed by equivalent stiffness and damping coefficients;
- The axial and torsional ‘spring-damper’ groups have no masses and mass moments of inertia;

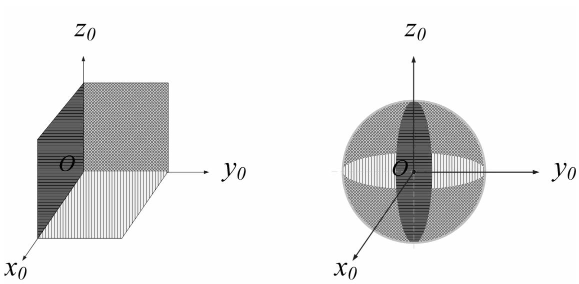

Fig. 4 Reference plane definition for MMET torsional elasticity by torsional ‘spring-damper’ groups

This discretised MMET system comprises a symmetrical and cylindrical double payload configuration, a cylindrical motor facility, and two axially flexible and essentially tubular tether sub-spans, as shown in Figure 3. The elasticity of the tether system is considered to be distributed symmetrically along each tether sub-span. The tether and the motor are connected by series ‘spring-damper’ groups. When the tether moves out of the orbital plane, the motor drive axis remains orthogonal to the spin plane, meanwhile, the motor torque will act about the principal axis through its centre of mass.

In the discretised non-planar tether model, environmental effects such as solar radiation, residual aerodynamic drag in low Earth orbit and electrodynamic forces, that may also influence the modelling, are reasonably assumed to be negligible in this context. The motor consists of a central rotor, which is attached to the propulsion tethers, and a stator which locates the rotor by means of a suitable bearing. The power supplies, control systems, and communication equipment are assumed to be fitted within the surrounding stator assembly in a practical installation. The stator also provides the necessary reaction that is required for the rotor to spin-up in a friction-free environment. The motor torque acts about the motor drive axis, and it is assumed here that the motor drive axis will stay normal to the spin plane of the propulsive tethers and payloads.

In order to describe the torsional elasticity clearly, three reference planes are defined in Figure 4. There are three orthogonal reference planes: $x_0 - O - y_0$, $x_0 - O - z_0$ and $z_0 - O - y_0$, which are located at the MMET’s COM. The modelling for the torsional elasticity is referenced onto the plane $x_0 - O - z_0$.

As shown in Figure 5, the tether length of the discretised MMET is from payload M_P to COM, where the time variant length $L(t)$ of the tether is the sum of L_0 and $L_x(t)$, the static length and the variable elastic length of the discretised tether, respectively. The axial elasticity behaviour is defined by the generalised coordinate L_x, and the axial elasticity modelling was given in [18] [19] [20].

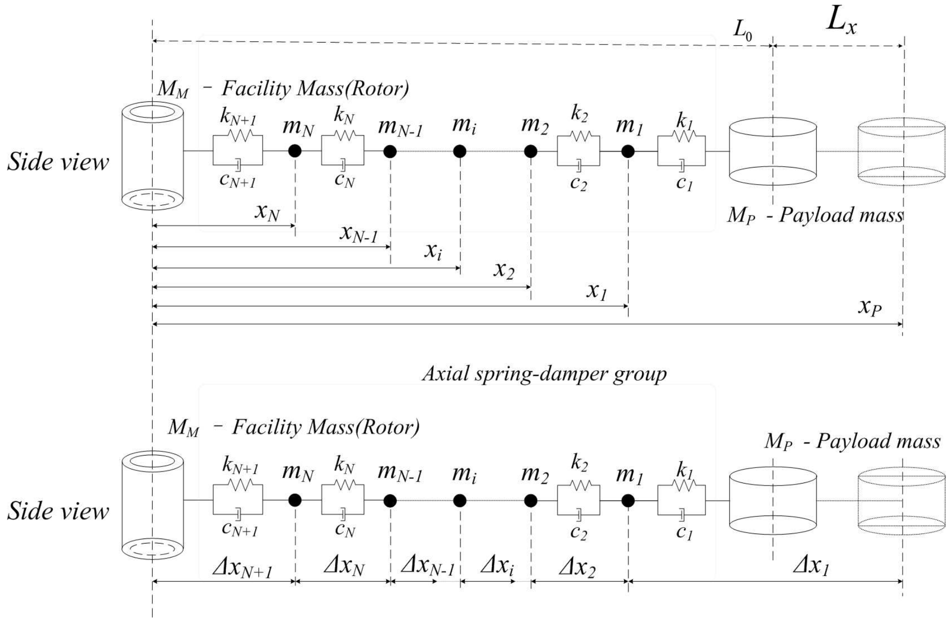

Fig. 5 Local absolute coordinate and local relative coordinate definitions for MMET axial elasticity

For the torsional elasticity modelling, as shown in Figure 6, the torsional elasticity is defined by a string of torsional 'spring-damper' groups (k_{ti}, c_{ti}), which connect the mass points of m_i in series with k_{t0} = k_{t1} = . . . = $k_{t(N+1)}$, c_{t0} = c_{t1} = . . . = $c_{t(N+1)}$, where i = $1, 2, \ldots, N+1$, the k_{t0} and c_{t0} are the default stiffness and damping coefficient values when in calculation, and N is the number of discretised mass points. All the torsional 'spring-damper' groups are defined on the plane $x_0 - O - z_0$ as shown in Figure 7. The t in the subscript means the torsional elastic parameter, and the generalised coordinate γ_x defines the equivalent torsional elasticity as shown in Figure 6, which is in addition to the solid body rolling generalised coordinate γ. The subscript 'x' means the generalised coordinate with elasticity.

There are seven generalised coordinates in this model [20], in the form of five rotational coordinates (ψ, θ, α, γ, γ_x) and two translational coordinates (L_x, R). Coordinate ψ defines the spin-up performance of the MMET system and is the 'in-plane pitch angle'. This denotes the angle from the x_0 axis in Figure 2 to the projection of the tether onto the orbit plane. θ is the circular orbit angular position, effectively the true anomaly. α is an out-of-plane angle, from the projection of the tether onto the orbit plane to the tether, and is always within a plane normal to the orbit plane. Generalised coordinate γ defines the solid body rolling angle, γ_x defines the torsional elastic effect, and lies between the torque plane and the tether spin plane. R is the distance from the Earth to the MMET COM, and L_x is the axial elastic length. The Lagrange equation is used to obtain the dynamical equations of motion based on the seven generalised coordinates.

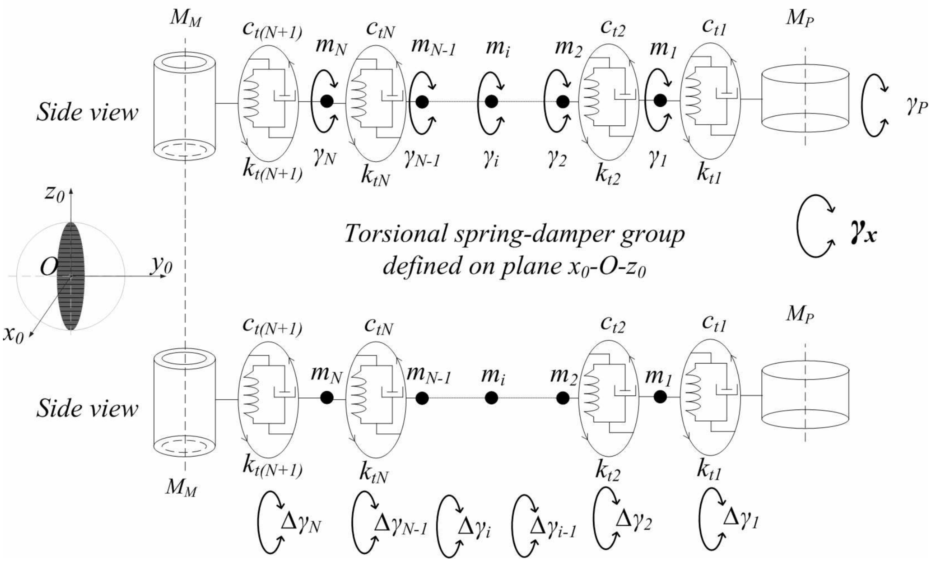

Fig. 6 Local absolute coordinate and local relative coordinate definitions for MMET torsional elasticity - reference onto the plane $x0 - O - z0$

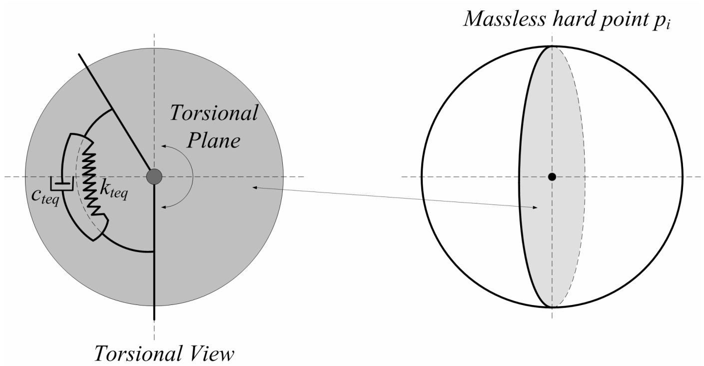

Fig. 7 Reference on the plane $x_0 - O - z_0$ for MMET torsional elasticity

Q_i are the generalised forces for the selected generalised coordinates q_i, ψ, γ_x and L_x, which are given in equations (1) - (3). As also shown in Table 1, the MMET system's kinetic energy is T, the potential energy is U.

Table 1 Axial and torsional elastic discretised MMET generalised coordinates and generalised forces

i	q_i	Q_i	T	U	Equations of Motion
1	ψ	(1)	(4)	(5)	(8)
2	γ_x	(2)			(9)
3	L_x	(3)			(10)

$$Q_\psi = FL\cos\gamma\cos\alpha = \tau\cos\gamma\cos\alpha \tag{1}$$

$$Q_{\gamma_x} = -c_{teqmi}\dot{\gamma_x} \tag{2}$$

$$Q_{L_x} = -c_{eqmi}\dot{L_x} \tag{3}$$

Based on the assumptions, the mass moment of inertia of each discretised mass point can be ignored, and then the discretised mass point m_i's kinetic energy, which relates to the ignored mass moments of inertia $I_{y_{m_i}} = 0$, can also be ignored. Thus, the MMET system's kinetic energy equation can be simplified as equation (4).

$$\begin{aligned} T = &\frac{1}{2}M_{P1}\left(\dot{x}_{P1}^2+\dot{y}_{P1}^2+\dot{z}_{P1}^2\right)+\frac{1}{2}M_{P2}\left(\dot{x}_{P2}^2+\dot{y}_{P2}^2+\dot{z}_{P2}^2\right)+\frac{1}{2}M_M\left(\dot{x}_M^2+\dot{y}_M^2+\dot{z}_M^2\right)+\\ &\left[\frac{1}{2}\left(M_{P1}+M_{P2}\right)\dot{L_x}^2+m_0\sum_{i=1}^{N}\dot{x_i}^2\right]+\frac{1}{2}\left(I_{y_{P1}}+I_{y_{P2}}\right)\dot{\gamma_x}^2+\\ &\frac{1}{2}A\rho L\left(\dot{x}_{T1}^2+\dot{y}_{T1}^2+\dot{z}_{T1}^2\right)+\frac{1}{2}A\rho L\left(\dot{x}_{T2}^2+\dot{y}_{T2}^2+\dot{z}_{T2}^2\right)+\\ &\left[\frac{1}{2}I_{z_{P1}}+\frac{1}{2}I_{z_{P2}}+I_{z_T}+\frac{1}{2}I_{z_M}\right]\left(\dot{\psi}+\dot{\theta}\right)^2+\left[\frac{1}{2}I_{x_{P1}}+\frac{1}{2}I_{x_{P2}}+I_{x_T}+\frac{1}{2}I_{x_M}\right]\dot{\alpha}^2+\\ &\left[\frac{1}{2}I_{y_{P1}}+\frac{1}{2}I_{y_{P2}}+I_{y_T}+\frac{1}{2}I_{y_M}\right]\dot{\gamma}^2 \end{aligned} \tag{4}$$

This MMET system's potential energy is given in equation (5), where μ is the product of the universal gravitational constant G with the Earth's mass.

$$\begin{aligned} U = &-\frac{\mu M_{P1}}{\sqrt{L^2+R^2+2LRcos\alpha cos\psi}}-\frac{\mu M_{P2}}{\sqrt{L^2+R^2-2LRcos\alpha cos\psi}}-\frac{\mu M_M}{R}\\ &-\sum_{i=1}^{N}\frac{\mu\rho AL}{N\sqrt{R^2+\left(\frac{(2i-1)L}{2N}\right)^2+\frac{(2i-1)RLcos\alpha cos\psi}{N}}}\\ &-\sum_{i=1}^{N}\frac{\mu\rho AL}{N\sqrt{R^2+\left(\frac{(2i-1)L}{2N}\right)^2-\frac{(2i-1)RLcos\alpha cos\psi}{N}}}+2SE \end{aligned} \tag{5}$$

where

$$SE = SE|_{axial} + SE|_{torsional} \tag{6}$$

$$CE = CE|_{axial} + CE|_{torsional} \tag{7}$$

In this discretised model, the potential energy is stored as the strain energy in the assumed spring elements. The strain energy SE is defined in equation (6) for each tether sub-span, which includes the $SE|_{axial}$ term for axial elasticity , and the $SE|_{torsional}$ term for torsional elasticity. For the symmetrical double-ended MMET system, the total strain energy is $2SE$ in equation (5).

The CE term is an assumed dissipation function based on Rayleigh damping for each tether sub-span, which involves the $CE|_{axial}$ term and $CE|_{torsional}$ term for axial dissipation and torsional dissipation, respectively.

By following the Lagrangian procedure, the following governing equations for the selected generalised coordinates q_i are listed in equations (8) to (9), for $q_1 = \psi$, $q_2 = \gamma_x$, and $q_3 = L_x$ as given in Table 1, in which the generalised forces are given in equations (1) to (3) for q_1 to q_3.

$$\left(\frac{\mu M_{P2}\left(L_0+L_x\right)\cos\alpha\left(\begin{array}{c}\sin(\theta+\psi)\left(R\cos\theta-\cos\alpha\cos(\theta+\psi)\left(L_0+L_x\right)\right)-\\ \cos(\theta+\psi)\left(R\sin\theta-\cos\alpha\sin(\theta+\psi)\left(L_0+L_x\right)\right)\end{array}\right)}{\left(\begin{array}{c}\left(\cos\theta R-\cos\alpha\cos(\theta+\psi)\left(L_0+L_x\right)\right)^2+\\ \left(-\sin\alpha\left(L_0+L_x\right)\right)^2+\left(R\sin\theta-\cos\alpha\sin(\theta+\psi)\left(L_0+L_x\right)\right)^2\end{array}\right)^{3/2}}+\frac{\cos\alpha\mu M_{P1}\left(L_0+L_x\right)\left(\begin{array}{c}\cos(\theta+\psi)\left(R\sin\theta+\cos\alpha\sin(\theta+\psi)\left(L_0+L_x\right)\right)-\\ \sin(\theta+\psi)\left(R\cos\theta+\cos\alpha\cos(\theta+\psi)\left(L_0+L_x\right)\right)\end{array}\right)}{\left(\begin{array}{c}\left(R\cos\theta+\cos\alpha\cos(\theta+\psi)\left(L_0+L_x\right)\right)^2+\left(\sin\alpha\left(L_0+L_x\right)\right)^2+\\ \left(R\sin\theta+\cos\alpha\sin(\theta+\psi)\left(L_0+L_x\right)\right)^2\end{array}\right)^{3/2}}\right)-$$

$$\left(M_{P1}-M_{P2}\right)\left(\begin{array}{c}\left(L_0+L_x\right)\left(\begin{array}{l}\sin\alpha\dot{\alpha}\left(\sin\psi\dot{R}-\cos\psi R\dot{\theta}\right)-\\ \cos\alpha\left(\cos\psi\dot{R}+R\sin\psi\dot{\theta}\right)\left(\dot{\theta}+\dot{\psi}\right)\end{array}\right)+\\ \cos\alpha\left(\cos\psi R\dot{\theta}-\sin\psi\dot{R}\right)\dot{L_x}\end{array}\right)+$$

$$\frac{1}{2}\left(\begin{array}{l}-2\cos\alpha\left(M_{P1}+M_{P2}\right)\left(2\sin\alpha\dot{\alpha}\left(\dot{\theta}+\dot{\psi}\right)-\cos\alpha\left(\ddot{\theta}+\ddot{\psi}\right)\right)L_0^2\\ +2\left(\begin{array}{c}\sin\psi\left(M_{P1}-M_{P2}\right)\left(\sin\alpha\dot{R}\dot{\alpha}-\cos\alpha\left(R\dot{\theta}\dot{\psi}+\ddot{R}\right)\right)+\\ \cos\psi\left(M_{P1}-M_{P2}\right)\left(\begin{array}{c}\cos\alpha\dot{R}\left(\dot{\theta}-\dot{\psi}\right)+\\ R\left(\cos\alpha\ddot{\theta}-\sin\alpha\dot{\alpha}\dot{\theta}\right)\end{array}\right)\\ -2\cos\alpha\left(M_{P1}+M_{P2}\right)\left(\begin{array}{c}2L_x\sin\alpha\dot{\alpha}\left(\dot{\theta}+\dot{\psi}\right)-\\ L_x\cos\alpha\left(\ddot{\theta}+\ddot{\psi}\right)-\\ \dot{L_x}\cos\alpha\left(\dot{\theta}+\dot{\psi}\right)\end{array}\right)\end{array}\right)L_0\\ +2\sin\alpha\left(M_{P1}-M_{P2}\right)L_x\dot{\alpha}\left(\sin\psi\dot{R}-\cos\psi R\dot{\theta}\right)-\\ 2\sin 2\alpha\left(M_{P1}+M_{P2}\right)L_x^2\dot{\alpha}\left(\dot{\theta}+\dot{\psi}\right)+\\ 2\cos\alpha\left(M_{P1}-M_{P2}\right)\left(\begin{array}{c}\left(\cos\psi R\dot{\theta}-\sin\psi\dot{R}\right)\dot{L_x}+\\ L_x\left(\begin{array}{c}\cos\psi\left(\dot{R}\left(\dot{\theta}-\dot{\psi}\right)+R\ddot{\theta}\right)-\\ \sin\psi\left(R\dot{\theta}\dot{\psi}+\ddot{R}\right)\end{array}\right)\end{array}\right)\\ +M_M r_M^2\left(\ddot{\theta}+\ddot{\psi}\right)+\\ \cos 2\alpha\left(M_{P1}+M_{P2}\right)L_x\left(2\left(\dot{\theta}+\dot{\psi}\right)\dot{L_x}+L_x\left(\ddot{\theta}+\ddot{\psi}\right)\right)+\\ \left(M_{P1}+M_{P2}\right)\left(\left(\ddot{\theta}+\ddot{\psi}\right)r_P^2+2L_x\left(\dot{\theta}+\dot{\psi}\right)\dot{L_x}+L_x^2\left(\ddot{\theta}+\ddot{\psi}\right)\right)\end{array}\right)=Q_\psi \tag{8}$$

$$2k_{teqmi}\gamma_x+\frac{1}{12}\left(M_{P1}+M_{P2}\right)\left(h_P^2+3r_P^2\right)\ddot{\gamma_x}=Q_{\gamma_x} \tag{9}$$

$$
\left(\begin{array}{l}
2k_{eqmi}L_x + \\
\dfrac{\mu M_{P2}\begin{pmatrix} -2\cos\alpha\cos(\theta+\psi)\left(\cos\theta R-\cos\alpha\cos(\theta+\psi)\left(L_0+L_x\right)\right) \\ -2\sin\alpha\left(-\sin\alpha\left(L_0+L_x\right)\right) \\ -2\cos\alpha\sin(\theta+\psi)\left(R\sin\theta-\cos\alpha\sin(\theta+\psi)\left(L_0+L_x\right)\right)\end{pmatrix}}{2\begin{pmatrix}\left(\cos\theta R-\cos\alpha\cos(\theta+\psi)\left(L_0+L_x\right)\right)^2+\left(-\sin\alpha\left(L_0+L_x\right)\right)^2 \\ +\left(R\sin\theta-\cos\alpha\sin(\theta+\psi)\left(L_0+L_x\right)\right)^2\end{pmatrix}^{3/2}} \\
+\dfrac{\mu M_{P1}\begin{pmatrix} 2\cos\alpha\cos(\theta+\psi)\left(\cos\theta R+\cos\alpha\cos(\theta+\psi)\left(L_0+L_x\right)\right) \\ +2\sin\alpha\left(\sin\alpha\left(L_0+L_x\right)\right) \\ +2\cos\alpha\sin(\theta+\psi)\left(R\sin\theta+\cos\alpha\sin(\theta+\psi)\left(L_0+L_x\right)\right)\end{pmatrix}}{2\begin{pmatrix}\left(\cos\theta R+\cos\alpha\cos(\theta+\psi)\left(L_0+L_x\right)\right)^2 \\ +\left(\sin\alpha\left(L_0+L_x\right)\right)^2 \\ +\left(R\sin\theta+\cos\alpha\sin(\theta+\psi)\left(L_0+L_x\right)\right)^2\end{pmatrix}^{3/2}}
\end{array}\right)
$$

$$
-\left(\begin{array}{l}
\frac{1}{2}\cos 2\alpha\left(M_{P1}+M_{P2}\right)\left(L_0+L_x\right)\left(\dot\theta+\dot\psi\right)^2 \\
+\cos\alpha\left(M_{P2}-M_{P1}\right)\left(\sin\psi\dot R-\cos\psi R\dot\theta\right)\left(\dot\theta+\dot\psi\right) \\
+\sin\alpha\left(M_{P2}-M_{P1}\right)\dot\alpha\left(\cos\psi\dot R+R\sin\psi\dot\theta\right) \\
+\frac{1}{2}\left(M_{P1}+M_{P2}\right)\left(L_0+L_x\right)\left(2\dot\alpha^2+\left(\dot\theta+\dot\psi\right)^2+2\left(\dot{\alpha_x}^2+\dot{\varphi_x}^2\right)\right)
\end{array}\right)
$$

$$
+\left(\begin{array}{c}
-\sin\alpha\left(M_{P1}-M_{P2}\right)\dot\alpha\left(\cos\psi\dot R+R\sin\psi\dot\theta\right) \\
+\cos\alpha\left(M_{P1}-M_{P2}\right)\left(\sin\psi\dot R\left(\dot\theta-\dot\psi\right)+\cos\psi\left(R\dot\theta\dot\psi+\ddot R\right)+R\sin\psi\ddot\theta\right) \\
+2\left(M_{P1}+M_{P2}\right)\ddot{L_x}
\end{array}\right)=Q_{L_x} \tag{10}
$$

3 Hybrid Fuzzy Sliding Mode Control Strategy

To make the necessary enhancement required to obtain the FαSMC method, a hybrid control law is introduced. This combines the fuzzy logic control with sliding mode control in which a sliding hyperplane surface is generated by use of a skyhook damping law. Meanwhile, because the chattering phenomenon is an acknowledged drawback of sliding mode control and is usually caused by unmodelled system dynamics, a special boundary layer is also proposed around the sliding surface to solve the chattering problem [36].

A flow diagram for the FαSMC, applying the SkyhookSMC approach, is given in Figure 8. The hybrid control effects of the FLC and the SkyhookSMC are combined by equation (11). In equation (11), α is a switching factor which balances the weight of the fuzzy logic control to that of the skyhook surface sliding mode control. Clearly, α = 0 represents SkyhookSMC, and α = 1 represents FLC, $\alpha \in$ [0,1].

$$
u|_{F\alpha SMC}=\alpha u_{FLC}+(1-\alpha)\,u_{SkyhookSMC} \tag{11}
$$

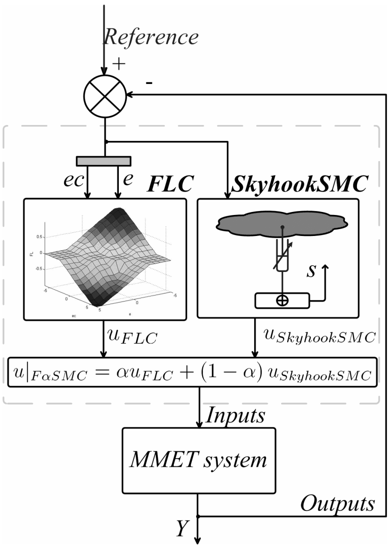

Fig. 8 FαSMC control flow diagram

3.1 Fuzzy Logic Controller

Fuzzy control is a practical alternative for a variety of challenging control applications since it provides a convenient method for constructing nonlinear controllers via the use of heuristic information. This may come from an operator who acts as a human-in-the-loop controller and from whom experiential data is obtained. The structure of the FLC for the MMET system is shown in Figure 9. An 'If-Then' rule base is then applied to describe the expert knowledge. The FLC rule base is characterised by a set of linguistic description rules based on conceptual expertise which arises from typical human situational experience. Table 2 is the 2-in-1-out FLC rule-base table which can drive the FLC inference mechanism, and this came from previous experience gained from examining dynamic simulations for tether length changes during angular velocity control. Briefly, the main linguistic control rules are as follows. (1) when the angular velocity(e) decreases, the tether length increases, conversely, when the angular velocity increases,the tether length decreases. (2) When the angular acceleration(ec) increases, the tether length increases can reduce the error between the velocity and the reference velocity, otherwise, when the angular acceleration decreases, the tether length decreases as well. A membership function (MF) is a curve that defines how each point in the input space is mapped to a membership value between 0 and 1. The MF for the MMET 7-DOF system is a Gaussian combination membership function. The inputs e and ec are the two input signals, and when interpreted from this fuzzy set, the full rule base is given in Table 2, which defines the relationship between the two fuzzified inputs of Error (E) and Change in Error (EC), with one output of the Fuzzified Length (FL), and the appropriate degree of membership as well [19].

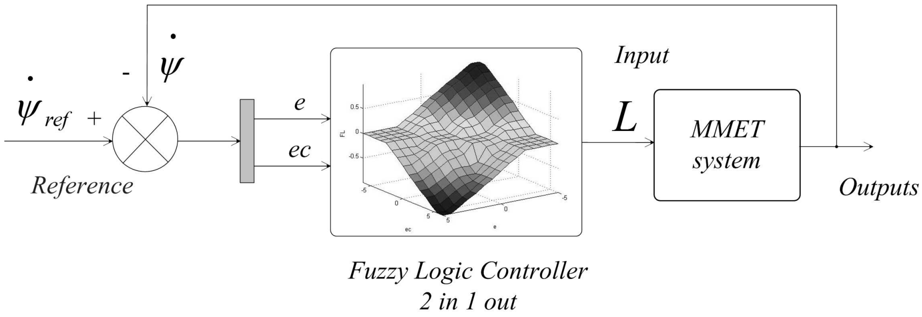

Fig. 9 FLC control flow diagram

Table 2 2-in-1-out FLC rule table for MMET 7-DOF

U		**EC**								
		NB	**NM**	**NS**	**NZS**	**ZE**	**PZS**	**PS**	**PM**	**PB**
	NB	NB	NM	NS	NZS	PZS	PZS	PS	PM	PB
	NM	NM	NM	NZS	NZS	PZS	PZS	PZS	PM	PM
	NS	NS	NS	NZS	NZS	PZS	PZS	PZS	PS	PS
	NZS	NZS	NZS	NZS	NZS	ZE	PZS	PZS	PZS	PZS
E	**ZE**	PZS	PZS	PZS	ZE	ZE	ZE	PZS	PZS	PZS
	PZS	PZS	PZS	PZS	PZS	ZE	NZS	NZS	NZS	NZS
	PS	PS	PS	PZS	PZS	PZS	NZS	NZS	NS	NS
	PM	PM	PM	PS	PZS	PZS	NZS	NS	NM	NM
	PB	PB	PM	PS	PZS	PZS	NZS	NS	NM	NB

3.2 Sliding Mode Control with Skyhook Surface

The objective of the SkyhookSMC controller is to consider the nonlinear MMET system as the controlled plant, and therefore defined by the general state space in equation (12):

$$\dot{x} = f(x, u, t) \tag{12}$$

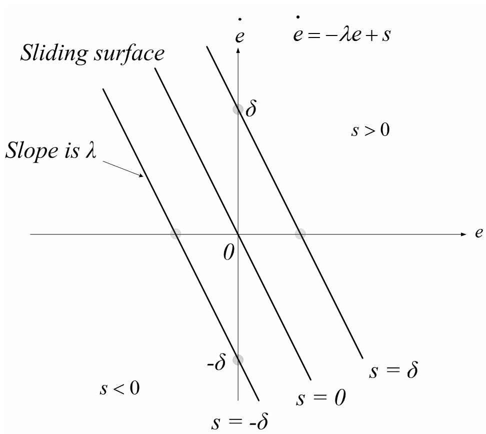

Fig. 10 Sliding surface definition

where $x \in R^n$ is the state vector, n is the order of the nonlinear system, $u \in R^m$ is the input vector, and m is the number of inputs. In the MMET system, we have $x = \{\psi, \dot{\psi}\}$, $u = \{L\}$. $s(e,t)$ is the sliding surface of the hyperplane, which is given in equation (13) and shown in Figure 10, where λ is a positive constant that defines the slope of the sliding surface.

$$s\left(e,t\right) = \left(\frac{d}{dt} + \lambda\right)^{n-1} e \tag{13}$$

The MMET system is a second-order system. Then, let n = 2 mean that it is a second-order system, in which s defines the position error (e) and velocity error ($\dot{e}$) in equation (14), $e = \{\dot{\psi} - \dot{\psi}_{Ref}\}$, where $\dot{\psi}_{Ref} = 0$ is the reference signal of angular velocity as shown in Figure 9.

$$s = \dot{e} + \lambda e = \ddot{\psi} + \lambda\dot{\psi} \tag{14}$$

From equations (13) and (14), the second-order tracking problem is now being replaced by a first-order stabilisation problem in which the scalar s is kept at zero by means of a governing condition. Obtained from the use of the Lyapunov stability theorem, the governing condition is given in equation (15), and it states that the origin is a globally asymptotically stable equilibrium point for the control system. Equation (16) is the negative definition, and it shows that the MMET's stable behaviour must be satisfied by the negative condition.

$$V\left(x,t\right) = \frac{1}{2}s^2 \tag{15}$$

$$\dot{V}\left(s\right) = s\dot{s} = \lambda^2 e\dot{e} + \lambda\left(\dot{e}^2 + e\ddot{e}\right) + \dot{e}\ddot{e} < 0 \tag{16}$$

The skyhook control strategy was introduced in 1974 by Karnopp et al. [37]. In Figure 11 the basic idea is to link a vehicle body's sprung mass to the 'stationary sky' by a controllable 'skyhook' damper, which can then reduce vertical vibrations due to all kinds of road disturbances. Skyhook control can reduce the resonant peak of the sprung mass quite significantly and thus can achieve a good ride quality in the car problem. By borrowing this idea to reduce the sliding chattering phenomenon, in Figure 12, a soft switching control law is introduced for the major sliding surface switching activity in equation (17), in order to reduce the chattering and to achieve good switch quality for the FαSMC combined with SkyhookSMC.

$$u_{SkyhookSMC} = \begin{cases} -c_0 \tanh\left(\frac{s}{\delta}\right) & s\dot{s} > 0 \\ 0 & s\dot{s} \leq 0 \end{cases} \tag{17}$$

where c_0 is an assumed positive damping ratio for the switching control law. This law needs to be chosen in such a way that the existence and the reachability of the sliding mode are both guaranteed. Note that δ is an assumed positive constant which defines the thickness of the sliding mode boundary layer [36].

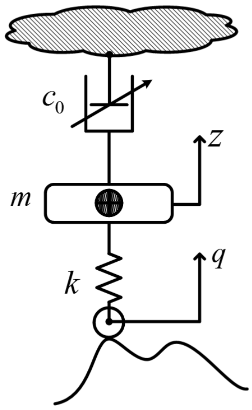

Fig. 11 Ideal skyhook damper

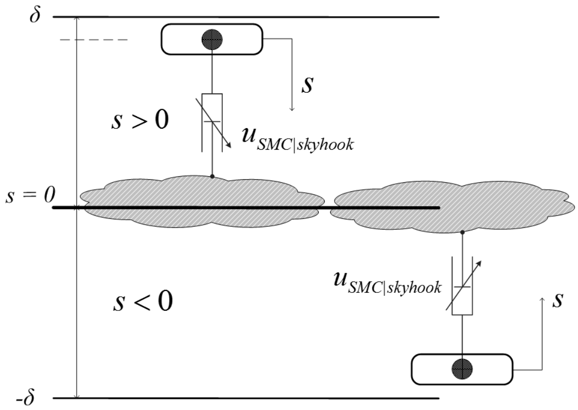

Fig. 12 Sliding skyhook surface definition

4 Simulations

Numerical results are obtained using a specially devised co-simulation toolkit of $MATLAB$ and $MATHEMATICA$ functions in an integrated programme to provide a new toolbox, known henceforth here as $SMATLINK$ [38]. This integrates the control in $MATLAB$ and the MMET modelling in $MATHEMATICA$. The difference between velocity and acceleration of ψ with the reference velocity and acceleration of ψ are selected as error and change-in-error feedback signals for the MMET system's spin-up control. Unless stated otherwise, all the results are generated using the parameters for the MMET system and controller in Table 3.

5 Conclusions

It is easy to switch the controller between the SkyhookSMC and the FLC modes when a proper value of α is selected $(0 < \alpha < 1)$, and the hybrid fuzzy sliding mode controller is generated combining FLC with a soft continuous switching SkyhookSMC law based on

Table 3 MMET 7-DOF system parameters

N	number of mass points	20
$\mu\,(m^3s^{-2})$	gravitational constant	3.98×10^{14}
$M_P\ (Kg)$	propulsion tether payload mass	1000
$M_M\ (Kg)$	mass of motor facility	5000
$r_{Tinner}\ (m)$	radius of tether inner tube	0.08
$r_{Touter}\ (m)$	radius of tether outer tube	0.1
$r_M\ (m)$	radius of motor facility	0.5
$r_P\ (m)$	radius of payload	0.5
r_{per}(m)	periapsis distance	6.89×10^6
$r_{apo}\ (m)$	apoapsis distance	1.034×10^7
$L_0\ (m)$	static length tether sub-span	50000
$A\,(m^2)$	undeformed tether tube cross-sectional area	1.1×10^{-2}
$\rho\,(kg/m^3)$	tether density	970
e	circular orbit with eccentricity	0.2
$\psi\ (rad)$	initial angular	0.0
$\dot{\psi}\ (rad/s)$	initial angular velocity	0.0
$\dot{\psi}_{ref}\ (rad/s)$	reference angular velocity	0.0
$\tau\ (Nm)$	motor torque	2.5×10^6
$c_i\ (Ns/m)$	tether sub-span axial damping coefficient	2×10^6
$k_i\ (N/m)$	tether sub-span axial stiffness	2×10^9
$c_{ti}\ (Ns/m)$	tether sub-span torsional damping coefficient	2×10^6
$k_{ti}\ (N/m)$	tether sub-span torsional stiffness	2×10^9
Ke	FLC scaling gains for e	1
Kec	FLC scaling gains for ec	1
Ku	FLC scaling gains for u	21000
α	FαSMC switching factor	$\{0, 0.5, 1\}$
c_0	SkyhookSMC damping coefficient	-3000
δ	thickness of the sliding mode boundary layer	0.8
λ	slope of the sliding surface	0.0014

equation (17). All the control methods have an effect on the spin-up of the MMET 7-DOF system from the given initial conditions. The FαSMC hybrid fuzzy sliding mode control system parameters require a judicious choice of the FLC scaling gains of $\{Ke, Kec\}$ for fuzzification, Ku is the defuzzification gain factor which is used to map the control force to the range that actuators can generate practically. Similarly, the SkyhookSMC damping coefficient c_0 is required to expand the normalised controller output force into a practical range. The thickness of the sliding mode boundary layer is given by δ, and the slope of the sliding surface by λ. Both data came from the previous MMET 7-DOF system spin-up simulation results without control, which are given in Table 3. In this simulation the FαSMC is used, with $\alpha = 0.5$ to balance the control weight between the FLC and the SkyhookSMC modes.

Different values of $\alpha = \{0.0, 0.5, 1.0\}$ can be used for $\{SkyhookSMC$, $F\alpha SMC$, $FLC\}$ control, respectively, of the MMET 7-DOF system. Figure 13 gives the time responses for the spin-up velocity $\dot{\psi}$, with different values of α. These results show that all the control methods have an effect on the spin-up of the MMET system from the given initial conditions.

Figures 14 and 15 give the axial and torsional elastic behaviour of the MMET in the simulation with the appearance of stable axial and torsional oscillation coupled with each other.

The phase plane plots with different values of α are shown in Figure 16 as limit cycles whose behaviour for the spin-up coordinate ψ clearly corroborates interpretations of steady state.

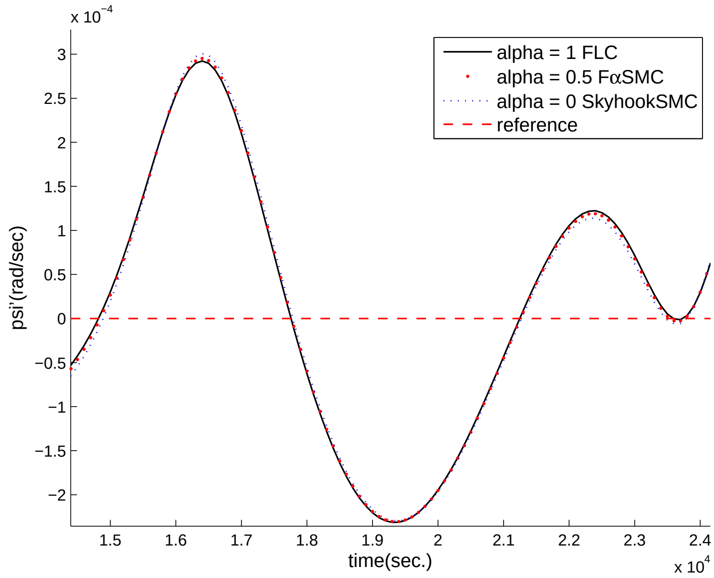

Fig. 13 Spin-up velocity with different values of α

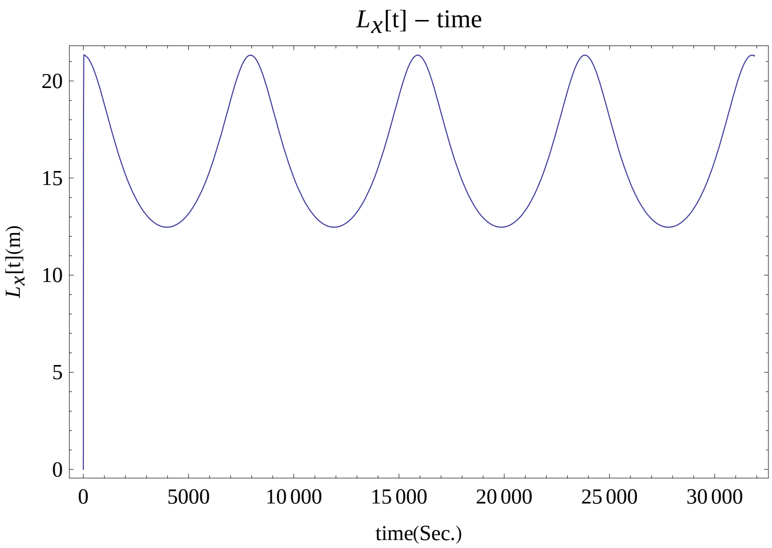

Fig. 14 MMET axial elastic behaviour

In Figure 17, the MMET spin-up error phase plane plots with different α are given, and they show that all the control methods offer limit cycles. The FLC caused generally faster response behaviour than the other two control methods for the spin-up coordinate ψ.

Figures 18 and 19 show the plots for the Lyapunov function and its derivative, showing the effect of FαSMC control for different values of α. SkyhookSMC has higher energy

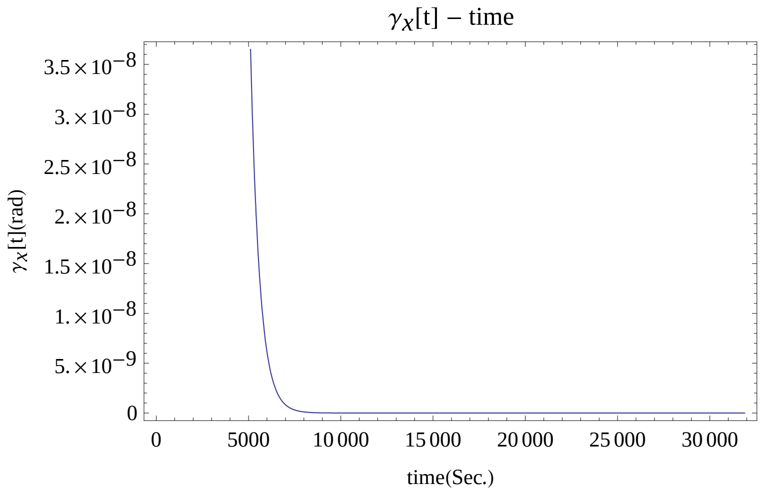

Fig. 15 MMET torsional elastic behaviour

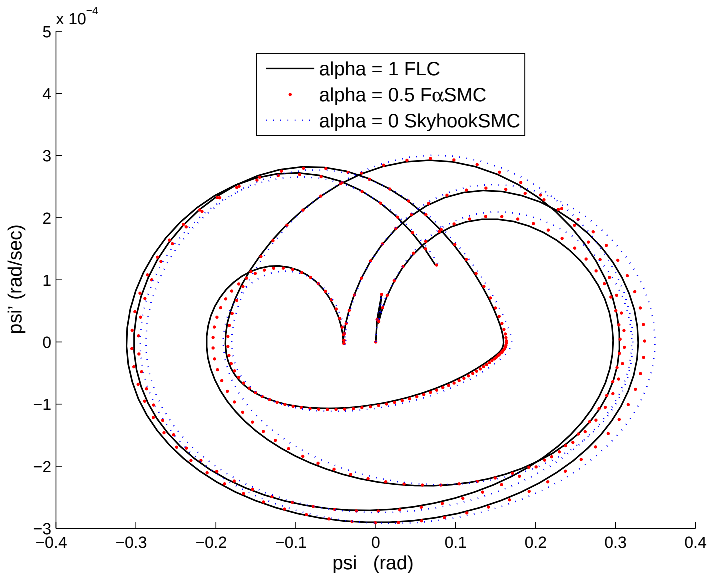

Fig. 16 MMET spin-up phase plane plots with different values of α

activities than the other two control methods, and FLC has the lowest associated energy around $V' = 0$, with FαSMC's energy in the middle of the three. FαSMC can balance the control effects of FLC and SkyhookSMC for stable MMET 7-DOF spin-up outputs and associated energy activities.

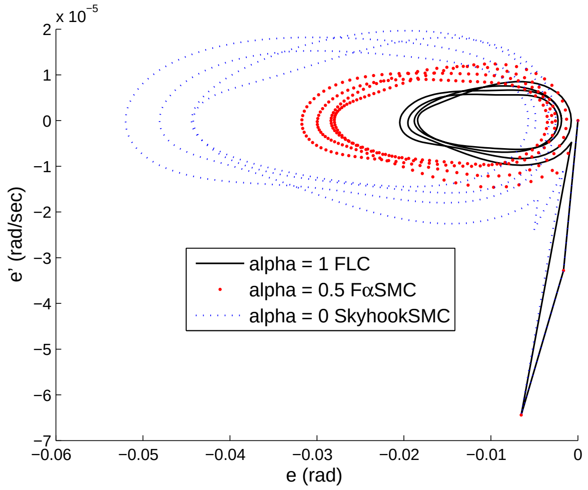

Fig. 17 MMET spin-up errors phase plane plots with different values of α

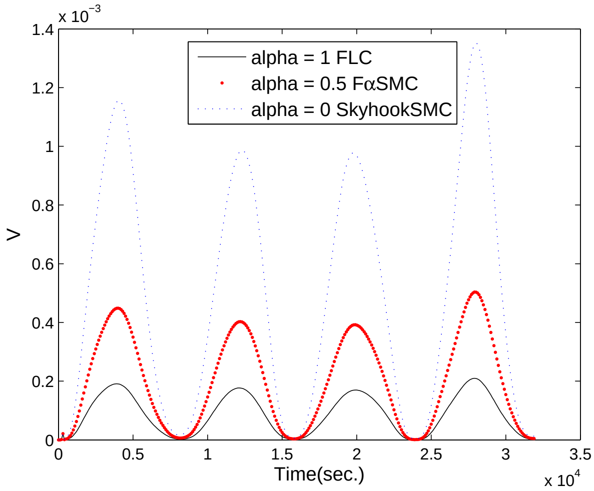

Fig. 18 Lyapunov function for spin-up control methods with different α

6 Future work

The work in this paper has shown that by including the switching factor α, the FαSMC hybrid controller can switch and combine control from FLC to the SkyhookSMC rapidly, according to design requirements. This can balance the weight of the FLC and SkyhookSMC to override spin-up enhancement for the MMET 7-DOF system. The parameter settings for the FαSMC need further consideration, because the current simulation results come from manual parameter tests. In order to enhance the parameter selection process and validation, some computational intelligence (CI) optimisation tools, such as genetic algorithms (GAs) and artificial neural networks (ANNs), could be applied for parameter selection for the FLC,

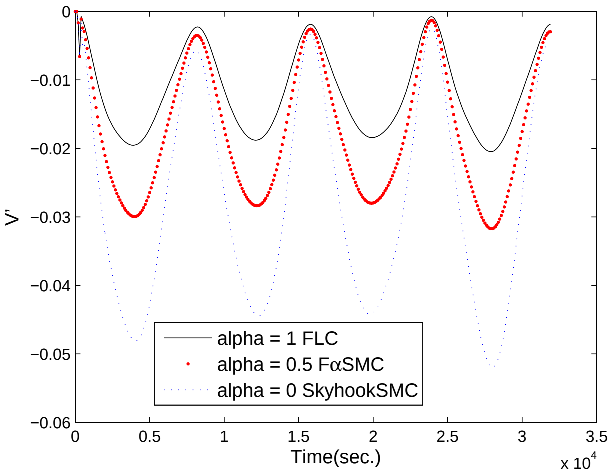

Fig. 19 time derivative of lyapunov function for spin-up control methods with different α

SMC, and FαSMC. This would give some useful reference sets for parameter settings. A GA has already been used as an optimisation tool for parameter selection of the MMET system when applied to payload transfer from low Earth orbit (LEO) to geostationary Earth orbit (GEO), and the GA's optimisation ability has, in that case, been reasonably demonstrated [39].

References

1. P.M. Bainum, V.K. Kumar, (1980) "Optimal Control of the Shuttle-Tethered-Subsatellite System", Acta Astronautica, Volume 7, Issue 12, Page 1333-1348.
2. K. Kumar, S. Pradeep, (1998), "Strategies for Three Dimensional Deployment of Tethered Satellites", Mechanics Research Communications, Volume 25, Number 5, September, Page 543-550.
3. S. Pradhan, V.J. Modi, A.K. Misra, (1999), "Tether-Platform Coupled Control", Acta Astronautica, Volume 44, Issue 5, Page 243-256.
4. J. F. Goulet, C. W. de Silva, V. J. Modi, A. K. Misra, (2001), "Hierarchical control of a space-based deployable manipulator using fuzzy logic", Journal of Guidance, Control, and Dynamics, Volume 24, Number 2, Page 395-405.
5. B. Barkow, (2003), "Controlled deployment of a tethered satellite system", PAMM, Volume 2, Issue 1, Page 224-225.
6. B. Barkow, A. Steindl, H. Troger, G. Wiedermann, (2003), "Various Methods of Controlling the Deployment of a Tethered Satellite", Journal of Vibration and Control, Volume 9, Number 1-2, Page 187-208.
7. B. Barkow, A. Steindl, H. Troger, (2005), "A targeting strategy for the deployment of a tethered satellite system", Journal of Applied Mathematics, 70:626-644.
8. V.J. Modi, J. Zhang, C.W. de Silva, (2005), "Intelligent Hierarchical Modal Control of A Novel Manipulator with Slewing and Deployable Links", Acta Astronautica, Volume 57, Issue 10, Page 761-771.
9. H. Gl$\ddot{a}\beta$el, F. Zimmermann, S. Br$\ddot{u}$ckner, U. M. Sch$\ddot{o}$ttle, S. Rudolph, (2004), "Adaptive Neural Control of the Deployment Procedure for Tether-Assisted Re-Entry", Aerospace Science and Technology, Volume 8, Issue 1, Page 73-81.
10. P. Williams, D. Sgarioto, P. Trivailo, (2006), "Optimal Control of an Aircraft-Towed Flexible Cable System", Journal of Guidance, Control, and Dynamics, Volume 29, Number 2, Page 401-410.
11. P. Williams, (2006), "Optimal Deployment/Retrieval of a Tethered Formation Spinning in the Orbital Plane", Journal of Spacecraft and Rockets, Volume 43, Number 3, Page 638-650.
12. P. Williams, (2006), "Libration control of tethered satellites in elliptical orbits", Journal of Spacecraft and Rockets, Volume 43, Number 2, Page 476-479.

13. S. Chung, J. E. Slotine, D. W. Miller, (2007). “Nonlinear model reduction and decentralized control of tethered formation flight by oscillation synchronization”, Journal of Guidance, Control, and Dynamics, Volume 30, Number 2, Page 390-400.
14. S. Chung, D. W. Miller, (2008), “Propellant-Free Control of Tethered Formation Flight, Part 1: Linear Control and Experimentation”, Journal of Guidance, Control, and Dynamics, Volume 31, Number 3, Page 571-584.
15. S. Chung, J. E. Slotine, D. W. Miller, (2008), “Propellant-free control of tethered formation flight, part 2: Nonlinear underactuated control”, Journal of Guidance, Control, and Dynamics, Volume 31, Number 5, Page 1437-1446.
16. M. P. Cartmell, (1998), “Generating Velocity Increments by Means of a Spinning Motorised Tether”, 34th AIAA/ASME/SAE/ASEE Joint Propulsion Conference and Exhibit, Cleveland Conference Center, Cleveland, Ohio, USA, AIAA-98-3739.
17. S.W. Ziegler, M. P. Cartmell, (2001), “Using Motorised Tethers for Payload Orbital Transfer”, Journal of Spacecraft and Rockets, Volume 38, Number 6, Pages 904-913.
18. Y. Chen, M.P. Cartmell, (2007), “Dynamical Modelling of the Motorised Momentum Exchange Tether Incorporating Axial Elastic Effects”, Advanced Problems in Mechanics, 20-28 June, Russian Academy of Sciences, St Petersburg, Russia.
19. Y. Chen, M.P. Cartmell, (2009), “Hybrid Fuzzy and Sliding-Mode Control for Motorised Tether Spin-Up When Coupled with Axial Vibration”, 7th International Conference on Modern Practice in Stress and Vibration Analysis, 8-10 September 2009, New Hall, Cambridge, UK.
20. Y. Chen, M.P. Cartmell, (2009), “Hybrid Sliding Mode Control for Motorised Space Tether Spin-up when Coupled with Axial Oscillation”, Advanced Problems in Mechanics, June 30-July 5, St Petersburg, Russia.
21. K. M. Passino , S. Yurkovich, (1998), “Fuzzy Control”, Addison Wesley Longman, Menlo Park, CA.
22. S. V. Emelyanov, (1967), “Variable Structure Control Systems (in Russian)”, Moscow: Nauka.
23. Y. Itkis, (1976), “Control Systems of Variable Structure”, New York: Wiley
24. V. A. Utkin, (1978), “Sliding Modes and Their Application in Variable Structure Systems”, Moscow: Nauka (in Russian) (also Moscow: Mir, 1978, in English).
25. A. Ishigame, T. Furukawa, S. Kawamoto, T. Taniguchi, (1991), “Sliding Mode Controller Design Based on Fuzzy Inference for Non-Linear System”, International Conference on Industrial Electronics, Control and Instrumentation, Kobe, Japan, 28 October-1 November, Volume 3, Pages 2096-2101.
26. A. Ishigame, T. Furukawa, S. Kawamoto, T. Taniguchi, (1993), “ Sliding mode controller design based on fuzzy inference for nonlinear systems”, IEEE Trans. Industrial Electronics, 40(1), 64-70.
27. C. Kung, W. Kao, (1998) “GA-based grey fuzzy dynamic sliding mode controller design”, The 1998 IEEE International Conference on Fuzzy Systems Proceedings, IEEE World Congress on Computational Intelligence, Anchorage, AK, USA, Volume 1, Pages 583-588.
28. P. C. Chen, C. W. Chen, W. L. Chiang, (2009) “GA-Based Fuzzy Sliding Mode Controller for Nonlinear Systems”, Expert Systems with Applications: An International Journal, Volume 36, Issue 3, Pages 5872-5879.
29. K. C. Ng, Y. Li, D. J. Murray-Smith, K. C. Sharman, (1995), “Genetic Algorithm Applied to Fuzzy Sliding Mode Controller Design”, First International Conference on Genetic Algorithms in Engineering Systems: Innovations and Applications, Galesia, 12-14 Sepetember, Page 220-225.
30. L. A. Zadeh, (1965) “Fuzzy Sets”, Information and Control, Volume 8, Number 3, Pages 338-353.
31. Y. Chen, (2009), “Skyhook Surface Sliding Mode Control on Semi-active Vehicle Suspension Systems for Ride Comfort Enhancement”, Engineering, Scientific Research Publishing, Volume 1, Number 1, pp. 23-32.
32. J.J.E. Slotine, W. P. Li, (1991), “Applied Nonlinear Control”, Prentice-Hall International.
33. B. O’Dell, (1997), “Fuzzy Sliding Mode Control: A Critical Review”, Oklahoma State University, Advanced Control Laboratory, Technical Report ACL-97-001.
34. S. G. Tzafestas ,G. G. Rigatos, (1999), “A Simple Robust Sliding-Mode Fuzzy-Logic Controller of the Diagonal Type”, Journal of Intelligent and Robotic Systems, Volume 26, Numbers 3-4 , Page 353-388.
35. E. H. Mamdani, (1977), ”Applications of fuzzy logic to approximate reasoning using linguistic synthesis”, IEEE Transactions on Computers, Volume 26, Number 12, Page 1182-1191.
36. J. E. Slotine, (1982), “Tracking Control of Nonlinear Systems Using Sliding Surfaces with Application to Robot Manipulations”, PhD Dissertation, Laboratory for Information and Decision Systems, Massachusetts Institute of Technology.
37. D. C. Karnopp, M. J. Crosby , R. A. Harwood, (1974), “Vibration Control Using Semi-Active Force Generators”, Journals of Engineering for Industry, Transactions of the ASME, 94:619-626.
38. Y. Chen, (2009), “Simple MATLAB and MATHEMATICA Link Laboratory Toolbox”, http://www.mathworks.com/matlabcentral/fileexchange/20573.
39. Y. Chen, M. P. Cartmell, (2007), “Multi-objective Optimisation on Motorised Momentum Exchange Tether for Payload Orbital Transfer”, IEEE Congress on Evolutionary Computation, 25-28 September, Page 987-993.

List of Figures

List of Tables